

# Residual Monte Carlo Treatment of Time Variable with Consistent LO Acceleration

Simon R. Bolding and Jim E. Morel

*Texas A&M University Nuclear Engineering Department,  
sbolding@tamu.edu, morel@tamu.edu*

## INTRODUCTION

Accurate solution to the thermal radiative transfer (TRT) equations is important in the high-energy, high-density physics regime, e.g., for inertial confinement fusion and astrophysics simulations. Moment-based hybrid Monte Carlo (MC) methods have demonstrated great potential for accelerated solutions to TRT problems. Such methods iterate between a high-order (HO) transport equation and a low-order (LO) system formulated with angular moments of the transport equation over a fixed spatial mesh. Physics operators that are too expensive for the HO solver to resolve directly, e.g., photon absorption and emission, are moved to the LO system. The lower-rank LO equations can be solved with Newton methods to allow for non-linearities in the LO equations to be efficiently resolved. The high-order (HO) problem is defined by the transport equation that models the photon radiation with sources defined by the previous LO solution. Solution to the HO problem is used to construct consistency terms that require the next LO solution to be consistent with the HO solution. These consistency terms preserve the accuracy of the MC solution method in the LO equations, upon nonlinear convergence of the outer iterations.

Previously, residual Monte Carlo (RMC) methods have been used to provide efficient solution to the HO transport problem [?, ?]; high-fidelity solutions, with minimal statistical noise, have been achieved for problems with slowly varying solutions resulting from optically-thick, diffusive regions. However, the results in these works used a backward Euler (BE) discretization for the time variable, which can inaccurately disperse radiation wave-fronts in optically thin problems. In this work, we extend on the work in [?] to include higher-accuracy treatment of the time variable in the radiation equations. The exponentially-convergent Monte Carlo (ECMC) algorithm [?] was modified to include integration of the time-variable; this includes the introduction of a doubly-discontinuous (DD) trial space representation in time. A new parametric closure of the LO equations, introducing additional time-closure consistency terms, was derived to capture the time accuracy of the HO ECMC simulations. The LO equations can preserve the accuracy of MC radiation transport treatment in time, with the same numerical expense of Backward Euler (BE) time discretized equations. We have derived the LO equations directly from the transport equation, such that, neglecting the linear-discontinuous (LD) finite-element (FE) spatial discretization of the LO equations, the HO and LO solutions are consistent upon convergence. Herein we briefly describe the HO and LO solvers. We present results for one-dimensional, grey test problems and compare accuracy and efficiency to the implicit MC (IMC) method [?], the standard MC solution method for TRT problems.

## THEORY

The 1D, grey TRT equations consist of the radiation and material energy balance equations, i.e.,

$$\frac{1}{c} \frac{\partial I(x, \mu, t)}{\partial t} + \mu \frac{\partial I(x, \mu, t)}{\partial x} + \sigma_a I(x, \mu, t) = \frac{1}{2} \sigma_a a c T^4(x, t) \quad (1)$$

$$\rho c_v \frac{\partial T(x, t)}{\partial t} = \sigma_a \phi(x, t) - \sigma_a a c T^4(x, t), \quad (2)$$

where physical scattering could optionally be included in Eq. (1). In the above equations  $x$  is the position,  $t$  is the time,  $\mu$  is the  $x$ -direction cosine of the angular intensity  $I(x, \mu, t)$ ,  $\sigma_a$  is the macroscopic absorption cross section ( $\text{cm}^{-1}$ ), and  $a$ ,  $c$ ,  $\rho$ , and  $c_v$  are the radiation constant, speed of light, mass density, and specific heat, respectively. The desired transient unknowns are the material temperature  $T(x, t)$  and the mean radiation intensity  $\phi(x, t) = \int_{-1}^1 I(x, \mu, t) d\mu$ . The mean intensity is related to the radiation energy density  $E$  by the relation  $E = \phi/c$ . The equations can be strongly coupled through the gray Planckian emission source  $\sigma_a a c T^4$ , which is a nonlinear function of temperature, and the absorption term  $\sigma_a \phi$ . In general, the material properties are a function of  $T$ .

In the HOLO context, the LO solver models the physical scattering and resolves the material temperature spatial distribution  $T(x)$  for each time step. The fully-discrete LO equations are based on algebraic manipulations of exact moment equations, formed over a spatial finite element mesh. The emission source is assumed BE in time to simplify equations, but the radiation variable is left in terms of time-averaged and end of time step unknowns. This is analogous to the approximation made in IMC. Angularly, the LO radiation equations are similar to  $S_2$  equations, with element-averaged consistency parameters that are analogous to a variable Eddington factor. The material energy equations are similar those that would exist from an LDFE discretization. Additional consistency parameters must be included to eliminate the auxiliary radiation unknowns in the time-variable, such that only time-averaged and known, previous time-step values exist. These equations have the same numerical complexity as time-discrete  $S_2$  equations. If the angular and time consistency parameters were estimated exactly, then the LO equations are exact, neglecting spatial discretization error. The consistency parameters are lagged in each LO solve, estimated from the previous HO solution for  $I^{n+1}(x, \mu)$ , as explained below. For the initial LO solve within a time step, the parameters are calculated based on the  $I^n(x, \mu)$ . The LO equations always conserve energy, independent of the accuracy of the consistency terms.

The solution to the LO system is used to construct a spatially LD representation of the emission sources on the right hand side of Eq. (??). This defines a fixed-source, pure absorber transport problem for the HO operator. This HO

transport problem represents a characteristic method that uses MC to invert the continuous streaming plus removal operator with an LD representation of sources. We will solve this transport problem using ECMC. The output from ECMC is  $\tilde{I}(x, \mu)$ , a space-angle LD FE projection of the exact solution for  $I(x, \mu)$ . This projection has minimal statistical noise due to the residual formulation used by the ECMC algorithm. Once computed,  $\tilde{I}(x, \mu)$  is used to directly evaluate the necessary LO consistency parameters for the next LO solve. Since there is a global, functional representation of the angular intensity, LO parameters are estimated using quadrature and do not require additional tallies. The HO solution is not used to directly estimate a new temperature at the end of the time step; it is only used to estimate the spatial and angular parameters in the LO solution, which eliminates typical operator splitting stability issues that require linearization of the emission source.

The process of performing subsequential HO and LO solves, within a single time step, can be repeated to obtain an increasingly accurate solution for  $\phi^{n+1}(x)$  and  $T^{n+1}(x)$ . Thus, the HOLO algorithm, for the  $n$ -th time step, is

1. Perform a LO solve to produce an initial guess for  $T^{n+1,0}(x)$  and  $\phi^{n+1,0}(x)$ , based on consistency terms estimated with  $\tilde{I}^n$ .
2. Solve the HO system for  $\tilde{I}^{n+1,k+1/2}(x, \mu)$  using ECMC, based on the current LO estimate of the emission and scattering sources.
3. Compute LO consistency parameters with  $\tilde{I}^{n+1,k+1/2}$ .
4. Solve the LO system using HO consistency parameters to produce a new estimate of  $\phi^{n+1,k+1}$  and  $T^{n+1,k+1}$ .
5. Repeat 2 – 4 until convergence is achieved.
6. Store  $\tilde{I}^n \leftarrow \tilde{I}^{n+1}$ , and move to the next time step.

where the superscript  $k$  denotes an outer HOLO iteration. The convergence criteria is based on successive LO solutions for  $\phi^{n+1}(x)$  and  $T^{n+1}(x)$ . The consistency terms force the HO and LO solutions for  $\phi^{n+1}(x)$  to be consistent to the order of the current HOLO iteration error.

### The LO System

To derive the LO equations, we reduce the dimensionality of Eq. (1) and Eq. (2) by taking spatial, angular, and temporal integrals. The spatial moments are taken over each spatial cell  $i$ :  $x \in [x_{i-1/2}, x_{i+1/2}]$ , weighted with the standard linear finite element basis functions. For example, the left moment operator is defined by

$$\langle \cdot \rangle_{L,i} = \frac{2}{h_i} \int_{x_{i-1/2}}^{x_{i+1/2}} b_L(x)(\cdot) dx, \quad (3)$$

where  $h_i = x_{i+1/2} - x_{i-1/2}$  is the width of the spatial element and  $b_L(x) = (x_{i+1/2} - x)/h_i$  is the FE basis function corresponding to position  $x_{i-1/2}$ . Angularly, the equations are integrated over the positive and negative half-range integrals of the equations. The angular integrals of the intensity are defined as  $\phi^\pm(x) =$

$\pm 2\pi \int_0^{\pm 1} \psi(x, \mu) d\mu$ . Thus, in terms of half-range quantities,  $\phi(x) = \phi^-(x) + \phi^+(x)$ . Finally, the equations are integrated over the  $n$ 'th time step  $t \in [t^n, t^{n+1}]$ .

An example derivation for one of the First, Eq. (1) is integrated over a time step. Then, pairwise application of the  $L$  and  $R$  (right) basis moments with the  $+$  and  $-$  half-range integrals to Eq. (1) ultimately yields four equations, for each cell. Due to space limitations, only the final form of one equation is given for reference as Eq. (??) in the appendix. The four degrees of freedom (DOF) over each cell  $i$  are  $\langle \phi \rangle_{L,i}^+$ ,  $\langle \phi \rangle_{R,i}^+$ ,  $\langle \phi \rangle_{L,i}^-$ , and  $\langle \phi \rangle_{R,i}^-$ . The angular consistency terms are defined by the half-range averages

$$\langle \mu \rangle_{L,i}^+ = \frac{\frac{2}{h_i} \int_0^1 \int_{x_{i-1/2}}^{x_{i+1/2}} \mu b_L(x) \psi(x, \mu) dx d\mu}{\frac{2}{h_i} \int_0^1 \int_{x_{i-1/2}}^{x_{i+1/2}} b_L(x) \psi(x, \mu) dx d\mu}. \quad (4)$$

The consistency terms for the  $R$  basis moment and  $\mu_{i\pm 1/2}^\pm$  face terms are defined similarly.

The four coupled equations over each cell for the four DOF are exact; they have not been discretized in any way. However, the consistency parameters (defined by Eq. (4)) are not known a priori, and there is no relation between the volume and face averaged quantities. In the HOLO context, the equations for unknowns at iteration  $m + 1$  use consistency parameters computed using Eq. (4) and the latest HO solution  $\tilde{\psi}^{m+1/2}$ . For the initial LO solve, all average  $\mu$  parameters are set to  $\pm 1/\sqrt{3}$ , yielding a solution equivalent to diffusion with Mark boundary conditions (i.e., an  $S_2$  solution). To close the LO system spatially, the usual LD upwinding approximation is used, which is consistent with the HO solution. For example, for Eq. (??), the face terms  $\mu_{i-1/2}$  and  $\phi_{i-1/2}$  terms are upwinded from the previous cell  $i - 1$  (or boundary condition); the terms at  $x_{i+1/2}$  are linearly extrapolated, computed using the  $L$  and  $R$  basis moments.

Summing the equations over all cells, the global LO eigenvalue problem is formed. In operator notation, the global system is

$$\mathbf{D}\Phi = \frac{1}{k_{\text{eff}}} \mathbf{F}\Phi, \quad (5)$$

where  $\Phi$  is the vector of unknown space-angle moments,  $\mathbf{D}$  represents streaming plus removal minus scattering, and  $\mathbf{F}\Phi$  is the fission source. The matrix  $\mathbf{D}$  is an asymmetric banded matrix with a bandwidth of seven, which can be directly inverted efficiently without need for inner source iterations. Eq. (5) is solved using inverse power iteration, i.e., given  $k_{\text{eff}}^{(0)}$  and  $\Phi^{(0)}$ ,

$$\Phi^{(l+1)} = \frac{1}{k_{\text{eff}}^{(l)}} \mathbf{D}^{-1} \mathbf{F}\Phi^{(l)}, \quad k_{\text{eff}}^{(l+1)} = k_{\text{eff}}^{(l)} \frac{\int v \Sigma_f \phi^{(l+1)} dx}{\int v \Sigma_f \phi^{(l)} dx}.$$

The  $l$  iteration indices here are independent of the HOLO iteration  $m$ . The above power iteration is repeated until  $k_{\text{eff}}^{(l)}$  and  $\mathbf{F}\Phi^{(l)}$  are converged.

## The ECMC High Order Solver

The transport equation to be solved by ECMC is given by Eq. (??). For the HOLO context, in operator notation, this equation is defined as

$$\mathbf{L}I^{m+1/2} = q^m \quad (6)$$

where  $I^{m+1/2}$  is the intensity based on the  $m$ -th LO estimate of  $q$ , which is the Planckian emission source using  $T^{n+1,m}$ . The continuous linear operator  $\mathbf{L}$  includes the streaming, removal, and time derivative on the left-hand side of Eq. (??).

To perform the residual MC algorithm, it is necessary to have a trial space representation of the solution in all variables. The intensity is represented in  $x$  and  $\mu$  with a standard LDFE representation [?]. A step, doubly-discontinuous (SDD) trial space is used to represent the intensity as a function of time. The trial space representation for  $I(x, \mu, t)$  is then

$$\tilde{I}(x, \mu, t) = \begin{cases} \tilde{I}^n(x, \mu) & t = t^n \\ \tilde{I}(x, \mu) & t \in (t^n, t^{n+1}) \\ \tilde{I}^{n+1}(x, \mu) & t = t^{n+1} \end{cases} \quad (7)$$

where we have used  $\tilde{I}$  to denote the time-averaged LDFE projection in  $x$  and  $\mu$  of the intensity over the interior of the time step; the beginning and end of time step projections are denoted  $\tilde{I}^n$  and  $\tilde{I}^{n+1}$ , respectively. There is a projection error in using the LDFE projection to represent the intensity between time steps. However, with sufficient noise reduction and mesh resolution, this should be an acceptable error compared to the large statistical noise of standard MC. The SDD trial space provides a projection for all the desired unknowns that result from time-integration of the transport equation to produce a balance equation, i.e., the time-averaged, end of time step, and previous time step intensities. Another benefit of this trial space is it allows for infrastructure for computing the residual from the time-discrete case analytically to be used directly.

To define the ECMC algorithm, the HOLO iteration indices  $m$  are dropped, noting that the LO estimated  $q^m$  remains constant over the entire HO solve. The  $i$ -th approximate solution to Eq. (6) is  $\tilde{I}^{(i)}$ , where  $i$  identifies the MC batch. The  $i$ -th residual is  $r^{(i)} = q - \mathbf{L}\tilde{\psi}^{(i)}$ , which with manipulation gives the error equation

$$\mathbf{L}(\psi - \tilde{\psi}^{(i)}) = \mathbf{L}\tilde{\epsilon}^{(i)} = r^{(i)} \quad (8)$$

where  $\psi$  is the exact solution and  $\tilde{\epsilon}^{(i)}$  is finite element representation, in space and angle, of the error in  $\tilde{\psi}^{(i)}$ . The above equation represents a second, fixed-source, pure absorber transport equation. The operator  $\mathbf{L}$  is inverted without discretization via MC to produce an estimate of the error in  $\tilde{\psi}^{(i)}$ , i.e.,  $\tilde{\epsilon}^{(i)} = \mathbf{L}^{-1}r^{(i)}$ . The projections of  $\epsilon$  and  $\psi$  onto the LD space-angle trial space are computed using standard volumetric path-length estimators. A generalization to the linear basis functions for tallies used to estimate census energy from IMC [?]. The estimators are weighted by appropriate basis functions to tally the zeroth and first moments, in  $x$  and  $\mu$ , of  $I(x, \mu)$  over each space-angle cell.

The ECMC algorithm is

1. Solve Eq. (6) to compute the MC projection of the angular flux onto the LD  $x - \mu$  trial space  $\tilde{\psi}^{(0)}$ .
2. Compute  $r^{(i)}$ .
3. Solve  $\tilde{\epsilon}^{(i)} = \mathbf{L}^{-1}r^{(i)}$
4. Compute  $\tilde{\psi}^{(i+1)} = \tilde{\psi}^{(i)} + \tilde{\epsilon}^{(i)}$
5. Repeat 2 – 4 until desired convergence of the angular flux is achieved.

Convergence is based on the estimated relative error in  $\tilde{\psi}^{(i)}$ , defined as  $\epsilon_{rel} = \|\tilde{\epsilon}^{(i)}\|_2 / \|\psi^{(0)}\|_2$ . Exponential convergence (with respect to the number of particles simulated) of  $\tilde{\epsilon}$  is obtained because with each inversion of  $\mathbf{L}$  a more accurate estimate of the solution is used to compute the new residual, decreasing the magnitude of the MC source  $r^{(i)}$ . If the statistical estimate of  $\tilde{\epsilon}$  is not sufficiently accurate, then the batches would diverge. Because the true angular flux does not in general lie within the LD trial space, the iterative estimates of the error will eventually stagnate. An adaptive  $h$ -refinement algorithm is used to allow the system to continue converging towards the exact solution. Because some regions of refined cells are relatively small, the probability of particles being sampled from those cells is very low. To resolve issues this causes, stratified sampling is used to sample the same number of source particles from each space-angle cell. Currently, the number of particles sampled in each cell remains constant throughout the HO solve.

## RESULTS AND ANALYSIS

We have simulated the following 1D, grey test problems to demonstrate the accuracy of the HOLO algorithm: a thin problem and a standard Marshak wave. We use the  $L_2$  measure of variance in the end of time step intensities to form a figure of merit as

### Optically Thin Problem

We modify the problem in the previous problem by increasing the absorption cross section to  $0.2 \text{ cm}^{-1}$ ; all other problem parameters are the same. Radiation temperatures at the end of the last time step are compared for IMC, HOLO-TC, and HOLO-BE in Fig. 1. The HOLO-TC and HOLO-BE results were generated with  $30 \mu$  cells, and all spatial meshes used 200 cells. At smaller time step sizes, the effects of mesh imprinting are slightly apparent in the HOLO-TC results, leading to more dispersion near the wave-front. For  $\Delta t = 0.005 \text{ sh}$ , there is good agreement between the HOLO-TC results and IMC. As in the previous problem, the HOLO-BE results do not accurately capture the wavefront location. IMC demonstrates substantial statistical noise in the equilibrium region.

Table. ?? compares computed FOM values for the census radiation energy densities, for the case of  $\Delta t = 0.0005 \text{ sh}$ . HOLO results were generated for the case of 1 and 2 batches, with the same total number of histories per time step. At low particle counts for the larger time step size, the HOLO-TC method demonstrates substantial noise. This is due to the trial space representation of the census particles at the

end of the time step being poorly estimated. For the 2 batch case, the estimate from the first batch leads to less error in the census estimate as the ECMC solves are simply solving for the deviation from the time-averaged quantity. The results for the case of 30,000 histories are plotted in Fig. ?? for the HO and LO solution. As demonstrated, there seems to have been some instabilities introduced into the LO equations through noise; sufficient sampling of the census must occur. At smaller time-steps there is an increase in statistical efficiency, however there has been a loss in accuracy due to an increase in projection error. In general, this is a balance that much be considered.

The accuracy of the HOLO-ECMC method was compared to a reference solution from IMC. This problem is thin enough that we expect IMC to be accuracy with sufficient particle histories. The reference solution is the average of 20 IMC simulations of  $20 \times 10^6$  histories, each with  $\delta t = 10^{-4}$  sh. The estimated value of  $\|s\|$  for the reference solution is 0.025%. The  $L_2$  norm of the error in cell-averaged mean intensities is computed at the end of the last time step, was computed. The average over 20 simulations is then computed to provide the metric

$$\|e\|^l = \left( \frac{\sum_{i=1}^{N_c} (\phi_i^{n+1,l} - \phi_i^{n+1,ref})^2}{\sum_{i=1}^{N_c} (\phi_i^{n+1,ref})^2} \right)^{1/2}, \quad (9)$$

where  $\phi_i^{n+1,l}$  is the cell-averaged scalar intensity at the end of the last time step from the  $l$ -th independent simulation. The sample mean of  $\|e\|$  from 20 independent simulations provides a metric for the accuracy of a particular simulation:

$$\overline{\|e\|} = \frac{1}{20} \sum_{l=1}^{20} \|e\|^l \quad (10)$$

The accuracy results for

### Marshak Wave Problem

It is important to demonstrate that the time closures are stable in a mix of optically thick and optically thin regions, and that the ECMC method is still efficient in such problems. Simulations were performed for the Marshak wave problem defined in Sec. ???. The time step size is linearly increased from 0.001 sh to a maximum step of 0.01 sh over the first 10 time steps; the last time step is adjusted to reach the desired simulation end time. It was found for this problem that it was necessary to use more than one batch for the HOLO-TC algorithm to stably converge. This is because in the case of a single batch particles must reach census to accurately estimate the next time step value. These results were generated using the implicit-like time closure.

Figure 2 compares the accuracy of IMC, HOLO-TC, and HOLO-BE. The solutions are plotted at  $t = 3$  sh, with  $10^6$  histories per time step for all simulations. As demonstrated, there is good agreement among the results. It is noted that this problem can be accurately modeled with the Backward Euler time discretization, but the MC time closure appears to be stable even in the mix of optically thick and thin regions. Table III compares sample statistics for IMC and the HOLO method

with continuous time treatment and with a BE discretization. As demonstrated, at the lower history count (300,000), the HOLO-TC algorithm demonstrates a greater variance. These results used the implicit like time closure.

Later on, we can include a table, even one that spans two columns such as Table IV.

## CONCLUSIONS

We believe that the doubly discontinuous trial space for the time variable suffers from the fact that you need a point-wise estimate of the flux in the time variable. Alternatively, the LDFE trial space could also include the time variable (i.e., it is linear in time). This has the added benefit that the slope can be estimated over the interior of the time-step, so all particle tracks contribute to the score. However, there is some additional truncation error as the end of time-step is an extrapolated quantity. We are investigating the use of the LD trial space, but it requires significant modifications to the sampling algorithm; these modifications will be required to extend to higher spatial dimensions, so they should provide an interesting tool. We plan to include results for the LD representation in time for the full paper.

## APPENDIX

Numbering in the appendix is different:

$$2 + 2 = 5. \quad (A.1)$$

and another equation:

$$a + b = c. \quad (A.2)$$

## ACKNOWLEDGMENTS

## REFERENCES

1. J. WILLERT, C. KELLY, D. KNOLL, and H. PARK, "A Hybrid Approach to the Neutron Transport k-Eigenvalue Problem using NDA-based Algorithms," M&C. Sun Valley, ID (2013).
2. J. PETERSON, *Exponentially Convergent Monte Carlo for the 1-D Transport Equation*, Master's thesis, Texas A&M (2014).
3. A. SOOD, R. A. FORSTER, and D. KENT PARSONS, "Analytical benchmark test set for criticality code verification," *Progress in Nuclear Energy*, **42**, 1, 55–106 (2003).

	$\phi_T(0)$	$\phi_T(10)$	$\phi_T(20)$	$\phi_D(0)$	$\phi_D(10)$	$\phi_D(20)$	$\rho$	$\varepsilon$	$N_{it}$
$c = 0.999$	0.9038	20.63	31.24	0.9087	20.63	31.23	0.2192	$10^{-7}$	15
$c = 0.990$	0.3675	13.04	24.7	0.3696	13.04	24.69	0.2184	$10^{-7}$	15
$c = 0.900$	0.009909	4.776	17.64	0.009984	4.786	17.63	0.2118	$10^{-7}$	14
$c = 0.500$	$6.069 \times 10^{-5}$	2.212	15.53	$6.213 \times 10^{-5}$	2.239	15.53	0.2068	$10^{-7}$	13

TABLE IV. This is an example of a really wide table which might not normally fit in the document.

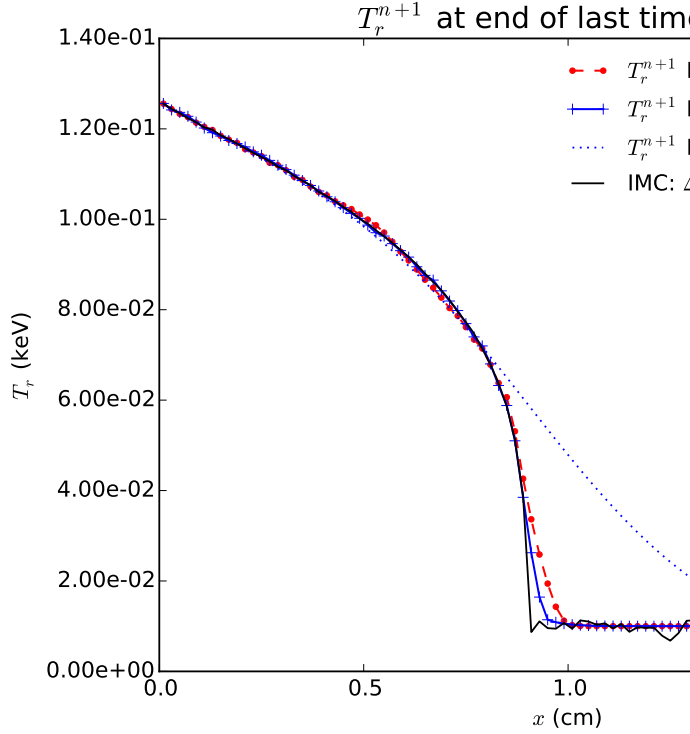


Fig. 1. Comparison of radiation temperatures of IMC and the HOLO method for different time step sizes and numbers of batches, for optically thin problem.

TABLE II. Comparison of sample statistics for the end of time step radiation energy densities, of the last time step, for the optically thin problem and  $\Delta t = 1 \times 10^{-4}$  sh. Simulation end time is  $t = 0.003$  sh.

hists./step	IMC	HOLO-TC (1)	HOLO-TC (3)	IMC	HOLO-TC (1)	HOLO-TC (3)
30,000	3.00%	0.55%	1.28%	1.00	29.8	71.8
300,000	0.96%	0.11%	0.30%	0.98	71.8	71.0
1,000,000	0.49%	0.06%	0.17%	1.11	71.0	71.0

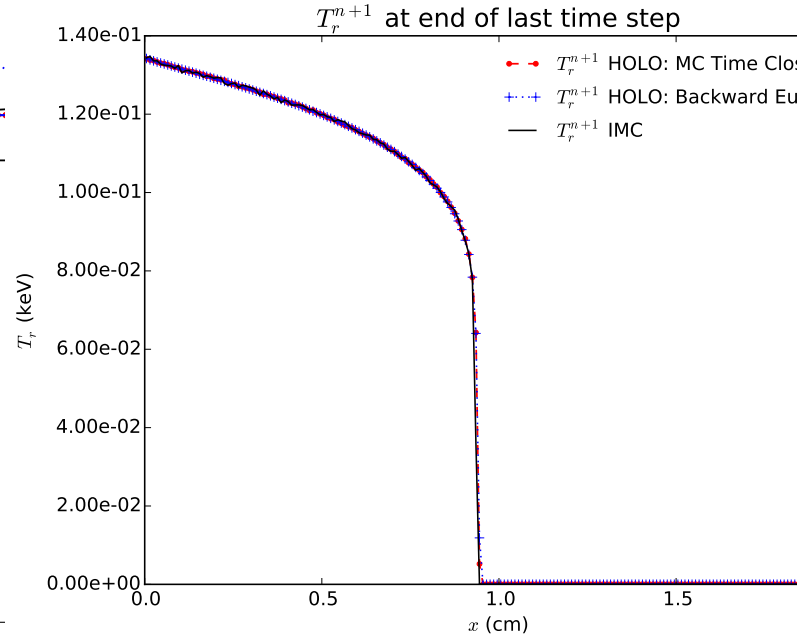


TABLE I. Comparison of sample statistics for the end of time step radiation energy densities, of the last time step, for the optically thin problem and  $\Delta t = 5 \times 10^{-4}$  sh. Simulation end time is  $t = 0.003$  sh.

hists./step	$\ s\ $			IMC	HOLO-TC (1)	HOLO-TC (3)
30,000	3.01%	18.29%	5.38%	1.00	1.00	1.65
300,000	0.99%	0.81%	0.74%	0.93	1.00	1.65
1,000,000	0.50%	0.30%	0.37%	1.10	3.42	2.0

TABLE III. Comparison of sample statistics for the end of time step radiation energy densities, of the last time step, for the optically thin problem, with  $10^6$  histories per time step.

TABLE III. Comparison of sample statistics for the end of time step radiation energy densities, of the last time step, for the marshak wave problem and maximum time step of 0.01 sh. Simulation end time is  $t = 3.0$  sh.

hists./step	$\ s\ $			FOM		
	IMC	HOLO-TC (2)	HOLO-BE (2)	IMC	HOLO-TC (2)	HOLO-BE (2)
300,000	2.25%	3.42%	0.30%	1.00	0.43	2050
1,000,000	1.27%	0.31%	0.17%	0.94	15.95	1806
Diamond Like Closure						
300,000	–	3.53%	–	–	0.41	–
1,000,000	–	0.37%	–	–	10.94	–